

Geodynamics & Space Geodesy

Geoscience studies are primarily conducted by the Geodynamics Branch and the Space Geodesy Branch. These groups study a broad range of subjects in geophysics, geology, and geodynamics, for both the Earth and solid planetary bodies. Observations using various techniques, especially space geodesy, magnetic field measurements, laser altimetry, and derivative models, are used to improve our understanding of solid-Earth interactions with the fluid envelopes at and above Earth's surface, as well as the evolution of the crust, mantle, and core. Major areas of work are described in more detail below. Examples of major accomplishments in the last year are provided in the following sections.

- (1) Gravity field model development for Earth and other planets, including both the static and time-varying components.
- (2) Analysis and modeling of the Earth's magnetic field and temporal changes in that field.
- (3) Effects of redistribution of geophysical fluids (air, water, ice) on the Earth and their manifestation in, for example, the time-variable gravity field and Earth rotation parameters.
- (4) Analysis and modeling of sea level variations in time and space relative to the precisely defined terrestrial reference frame.
- (5) Motions of the Earth's crust and their relationship with earthquake hazards, especially in areas of active subduction, and vertical changes indicated by paleolake levels.
- (6) Oceanic and solid body tidal processes and the resultant

deformation of the Earth, and influences on Earth rotation and gravity.

- (7) Long term orbital-rotational evolution on planetary objects such as Pluto, Triton, and Earth, as well as Earth's orbital-rotational relationship to long term climate change.
- (8) Magnetic properties of planetary crusts and the nature of sources of magnetic anomalies on both the Earth and Mars.
- (9) Topographic characterization of the surface of the Earth and Mars, in the former case to understand landforms associated with active faulting and earthquake hazard, and in the latter case to understand volcanic and tectonic structures in addition to origin and evolution of the fundamental crustal dichotomy.
- (10) Simulation of dynamics of the core fluid motions, how they relate to geomagnetic field and its variations, and surface geodetic observables.

The observational data that are analyzed and built into geophysical models come from various space geodetic and satellite magnetic measurements. These include satellite laser-ranging, Very-Long-Baseline Interferometry, Global Positioning System, and space-borne magnetometers. Determination of the precise orbits for Earth satellites and planetary spacecraft are performed via the software GEO-DYN. The Laboratory also develops new space techniques and algorithms that enable new measurements and solutions of the above-mentioned geodetic observables.

Lidar Mapping Reveals Pacific Northwest Seismic Hazards

More than 10,000 km² of high-resolution, public-domain topography data acquired by commercial airborne lidar mapping for the Puget Sound Lidar Consortium (PSLC) is revolutionizing investigations of active faulting, landslides, continental glaciation, and surficial processes in the seismically active Puget Lowland region of Washington State (Figure 1). The cover article of the June, 2003 issue of *GSA Today*, which reports on the PSLC effort, was requested by the Geological Society of America to highlight results pertinent to the Seattle area where the 2003 GSA annual meeting was held. The article is authored by Ralph Haugerud of the USGS, David Harding of the Lab for Terrestrial Physics, and additional members of the PSLC.



Figure 1. Location of Puget Sound Lidar Consortium mapping (green), and Puget Lowland fault zones (dashed grey).

The Puget Lowland—the population and economic center of the Pacific Northwest—presents special problems for hazards investigations, with its young glacial topography, dense forest cover, and urbanization. Lidar mapping during leaf-off conditions has led to a detailed digital model of the landscape beneath the forest canopy. The surface thus revealed contains a rich and diverse record of previously unknown surface-rupturing faults, Holocene and Pleistocene shoreline terraces documenting land surface elevation changes relative to sea level, deep-seated landslides, and glacial features.

The lidar mapping is accomplished using a small-footprint, multiple discrete return, scanning laser altimeter system operated by TerraPoint, LLC, following data specifications established by Harding and Haugerud. A nominal density of one laser pulse per square meter produces a densely sampled lidar point cloud. The discrete returns are classified as being from

ground, vegetation, or buildings, based on spatial filtering, from which high-resolution digital elevation models of the first-return surface (essentially a canopy top model) and the "bald Earth" (vegetation and buildings removed) are derived.

More than half a dozen suspected postglacial fault scarps have been identified by the lidar mapping (Figure 1). Five scarps that have been examined in detail by trenching show evidence of large, Holocene, surface-rupturing earthquakes. Carbon dating of organic material on fault surfaces exposed by the trenching documents that repeated earthquakes have occurred during the last 10,000 years. In addition, the lidar mapping enables detailed measurements of shoreline terrace elevations that record the amount of surface uplift produced by the earthquakes, and the discovery of previously unrecognized landslides, many likely generated by earthquake ground shaking (Figure 2). Information on the location, age, offsets, and magnitudes of these newly documented earthquakes and on the resulting distribution of surface deformation and landslides is redefining our understanding of the seismic hazard threatening this populous region.

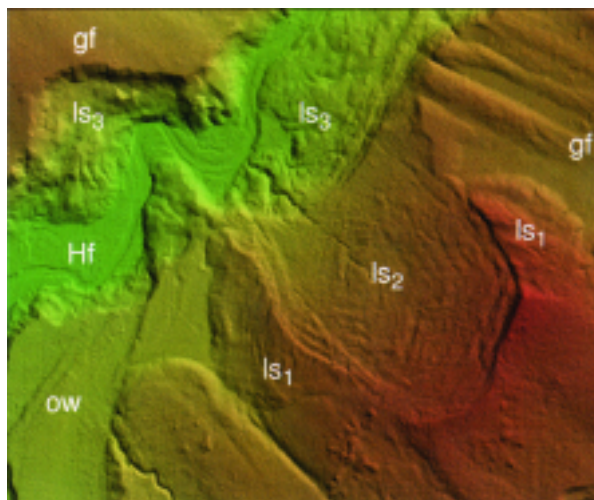


Figure 2. Landslides revealed in shaded relief lidar image of ground topography beneath vegetation, with colors from green to red representing increasing elevation. View is 3.5 km wide and the grid spacing is 1.8 m. Geomorphic units are gf—glacially fluted surface; ow—glacial outwash surface; ls—landslide, 1 (oldest) to 3 (youngest); Hf—Holocene fluvial surface.

Contact: David Harding, David.J.Harding@nasa.gov

Glacier Ice Mass Fluctuations and Fault Instability in Tectonically Active Southern Alaska

Across southern Alaska, the northwest directed subduction of the Pacific plate is accompanied by accretion of the Yakutat terrane to continental Alaska. This has led to high tectonic strain rates and dramatic topographic relief of more than 5000 meters within 15 km of the Gulf of Alaska coast. The glaciers of this area are extensive and include large glaciers undergoing wastage (glacier retreat and thinning) and surges. The large glacier ice mass changes perturb the tectonic rate of deformation at a variety of temporal and spatial scales. As summarized in the Global and Planetary Change, "Ice Sheets and Neotectonics", topical volume (in press, 2004), we estimated surface displacements and stresses associated with ice mass fluctuations and tectonic loading by examining GPS geodetic observations and numerical model predictions. Although the glacial fluctuations perturb the tectonic stress field, especially at shallow depths, the largest contribution to ongoing crustal deformation is horizontal tectonic strain due to plate convergence. Tectonic forces are thus the primary force responsible for major earthquakes. However, for geodetic sites located < 10-20 km from major ice mass fluctuations, the changes of the solid Earth due to ice loading and unloading are an important aspect of interpreting geodetic results.

The ice changes associated with Bering Glacier's most recent surge cycle are large enough to cause discernible surface displacements. Additionally, ice mass fluctuations associated with the surge cycle can modify the short-term seismicity rates in a local region. For the thrust faulting environment of the study region a large decrease in ice load may cause an increase in seismic rate in a region close to failure whereas ice loading may inhibit thrust faulting.

Prior to the 1979 St. Elias earthquake ($M=7.2$, star in Figure 1), the main thrust zone below the study region had been locked since the 1899 earthquakes and strain had been accumulating. During this same time period ongoing wastage of southern Alaska glaciers was 100's of meters up to almost 1 km. We used estimates of ice thickness decrease to calculate the changes in the fault stability margin around the region of the 1979 St. Elias earthquake and aftershocks. Our results suggest that the cumulative decrease in the fault stability margin due to ice wastage between 1899 and 1979 was large and would promote thrust faulting. Since earthquake hazard evaluations are based on the paleoseismic history of the region, for glaciated areas the concurrent glacial history should be considered in this evaluation.

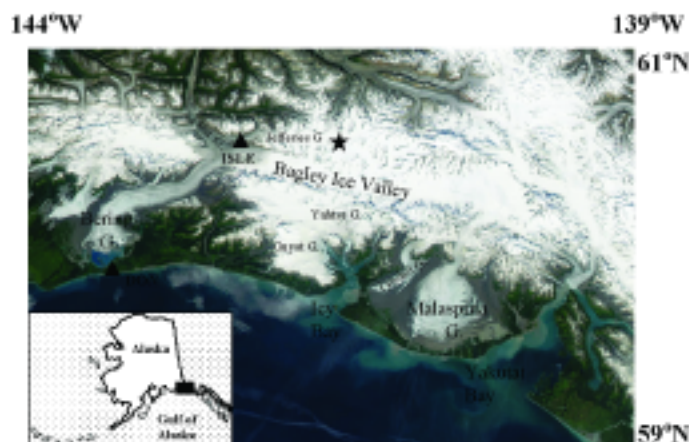


Figure 1. The August 9, 2003 true color, Moderate Resolution Imaging Spectroradiometer (MODIS) image from NASA's Aqua satellite of the southern Alaska coastal region. The image is courtesy of the MODIS Rapid Response Project at NASA/GSFC. The inset in the lower left hand corner shows the region of Alaska covered by Figure 1.

Crustal Deformation at the Arequipa Satellite Laser Ranging Observatory

The tectonically driven motion of the Arequipa SLR station changed significantly after a sequence of large earthquakes off the Peruvian coast. The main event on June 23, 2001, with magnitude greater than $M=8$, shifted the station by over 50 cm., which would release a strain built up over nearly forty years at the average pre-seismic rate. The Arequipa Satellite Laser Ranging station occupies an important position on the Altiplano of the Central Andes, 200 km from the margin of the oceanic Nazca plate subducting beneath the South American continental plate, and about 100 km from the coast. The behavior of this station is of particular interest in our analysis of SLR observations for reference frame maintenance and Earth orientation definition as Arequipa had been adopted as a fiducial site.

The observatory was established in 1970 as a component of the Smithsonian Astronomical Observatory (SAO) network and was ready to track the LAGEOS-I satellite immediately after its launch in May 1976. The SAO instrument up-grade program equipped the original ruby-laser system with pulse choppers in 1978 and further improvements in 1980 to reduce the original 50 cm range noise level to less than 10 cm. The evolution of the global laser tracking network in response to the goals of the MERIT program and the continuous improvements made through the upgrade programs of the contributing systems produced data quality at Arequipa at the level of about 5 cm in the mid-1980s. The station's performance was improved to 2 cm precision in 1990 when the TLRS-3 instrument developed at Goddard Space Flight Center replaced the SAO system. A further advance in station positioning capability was made in October 1992, when the LAGEOS-II satellite was launched, providing improved geometry and corresponding positioning resolution.

The generally accepted geophysical model for global plate motion, NUVEL-1A has the Nazca plate subducting beneath a South American continent assumed rigid with a rate of 77 mm/year and azimuth 79° east of north at the trench (17°S , 285°E). A decade of early SLR observations from the Arequipa station to the LAGEOS satellite indicated deformation in the region as the over-riding plate absorbed some of the eastward motion of the subducting material. The westward motion of the South American plate was attributed to the deceleration of the African plate's northeastward motion 30 million years ago through the coupling of general mantle circulation. The combination of observations of Nazca-South America convergence across the central Andes suggested that roughly half of the overall convergence could be released in future earth-

quakes, and supported the evidence that the Andes are continuing to build.

The sequence of events commencing with the $M=8.1$ event on June 23, 2001 caused a massive westward horizontal shift of 53 cm at Arequipa, which was followed by a further centimeter-level displacement during the $M=7.5$ aftershock on July 7.

The velocity of the station also changed after the 2001 events: the eastward motion relative to the South American Plate (15 mm/yr at 77° east of north) detected by almost twenty years of SLR observations prior to June, 2001, changed to the westward trend (33 mm/yr at 132° west of north). Two and a half years after the earthquakes, the direction of the station's motion continues to display a significant post-seismic relaxation signal in the horizontal component.

Kreemer and Holt noted the deviation of this and other space-geodetic observatories from the rigid plate assumptions of NUVEL-1A and proposed an alternative no-net-rotation model accommodating zones of diffuse deformation. The application of observations from stations whose motion conforms neither to a plate motion model nor to uniform motion requirements will present a growing challenge to robust reference frame definition as improved observations expose more subtle variations in the current space geodetic network.



Figure 1. Main shock displacement of the Arequipa SLR site.

Contact: Ronald Kolenkiewicz, Ronald.Kolenkiewicz-1@nasa.gov

Crustal Dynamics Data Information System (CDDIS)

The CDDIS is a dedicated data center supporting the international scientific community as NASA's space geodesy data archive since 1982. This data archive was initially conceived to support NASA's Crustal Dynamics Project; since the end of this successful program in 1991, the CDDIS has continued to support the science community through NASA's Solid Earth and Natural Hazards program, HQ Code YS. The CDDIS provides easy and ready access to a variety of data sets, products, and information about these data. The CDDIS archive includes Global Positioning System (GPS), GLObal NAVigation Satellite System (GLONASS), Satellite Laser Ranging (SLR), Very Long Baseline Interferometry (VLBI), and Doppler Orbitography and Radiolocation Integrated by Satellite (DORIS) data and products. The specialized nature of the CDDIS lends itself well to enhancement to accommodate diverse data sets and user requirements. Information about the system is available at <http://cddisa.gsfc.nasa.gov>.

The CDDIS serves as one of the primary data centers for the following services within the International Association of Geodesy (IAG):

- International GPS Service (IGS) and its diverse pilot projects and working groups
- International Laser Ranging Service (ILRS)
- International VLBI Service for Geodesy and Astrometry (IVS)
- International Earth Rotation and Reference Systems Service (IERS)
- International DORIS Service (IDS)

The CDDIS is operational on a dedicated computer facility located in Building 33 at NASA GSFC. This computer facility hosts web sites for the CDDIS, the ILRS, and several other GSFC facilities. The majority of the CDDIS data holdings are accessible through anonymous ftp and the web.

By the end of 2003, users had downloaded nearly 60 million files, averaging over 450 Gbytes in size each month. Furthermore, nearly 2000 distinct hosts users accessed the CDDIS on a monthly basis to download data. Users from over 100 countries accessed and downloaded data from the CDDIS last year. Over 130 institutions in over sixty countries supply data to the CDDIS on a daily basis for archival and distribution to the international user community.

CDDIS Activities in 2003

In support of the IGS pilot project on Low Earth Orbiter (LEO) missions, the CDDIS enhanced its archive to include GPS data from additional flight receivers (Jason-1). Analysts retrieved these data to produce precise orbits of these LEO platforms, which will aid in the generation of other products, such as temperature and water vapor profiles in the neutral atmosphere and ionosphere imaging products.

An updated archive structure for IDS data and products was implemented at the CDDIS.

The CDDIS staff assisted in the publication of several ILRS documents, particularly the proceedings from the 13th International Workshop on Laser Ranging and the 2002 ILRS annual report.

Staffing and Funding

The CDDIS staff consists of one civil servant and 2.5 Raytheon ITSS contractors.

Future Plans

A new LINUX-based (and backup) system was purchased in 2003 to replace the current UNIX server. This system has been configured with nearly 3 Tb of RAID disk space and a dedicated tape backup system. Plans are to have this system operational as the main CDDIS on-line server in mid-2004.

ICESat Calibration and Validation: Geodesy

The accurate geolocation of a laser altimeter's surface returns (the spots from which the laser energy reflects on the Earth's surface) is a critical issue in the scientific application of these data. The geolocation of the laser surface return is computed from the laser-altimeter surface range observations along with the precise knowledge of the spacecraft position, instrument tracking points, spacecraft attitude, laser pointing and observation times. These data have errors, and their pre-launch parameter values and models must either be verified or more likely corrections must be estimated once the instrument is on orbit. ICESat is no exception and pointing, ranging and timing corrections must be calibrated and validated post-launch. Towards this end, members of the Laboratory for Terrestrial Physics Space Geodesy Branch are participating in calibration and validation of ICESat data products, focusing on geodetic aspects of the mission.

An Integrated Residual Analysis (IRA) capability has been developed in order to support the calibration of spaceborne laser altimeter on-orbit biases, and to validate and improve mission orbit and geolocation solutions. In the IRA approach, orbit and instrument parameters (pointing, ranging and timing) can be simultaneously estimated from a combined reduction of laser range and spacecraft tracking data. The IRA capability was initially developed and tested using data from the two Shuttle Laser Altimeter (SLA) orbital missions and the Mars Global Surveyor (MGS) laser altimeter with support from the SLA, MGS, Vegetation Canopy Lidar, and ICESat projects.

At the core of the integrated residual analysis is Goddard Space Flight Center's GEODYN precise orbit and geodetic parameter estimation system. The laser altimeter range measurement model algorithms have been implemented within the GEODYN system. Therefore, the laser altimeter range processing can take advantage of GEODYN's reference frame modeling, geophysical modeling and its formal estimation process.

Input data includes range residuals at dynamically adjusted crossovers, and direct altimeter range observations with respect to a Mean Sea Surface model as well as with respect to high resolution Digital Elevation Models of selected land reference targets. Additional inputs are Global Positioning System and Satellite Laser Ranging tracking of the spacecraft, and orientation data from the GLAS Stellar Reference System and the mission Precision Attitude Determination.

Results of the IRA analysis during early operation of ICESat have been very successful, calibrating complex time-varying pointing variation at the arc-second accuracy level (Figures 1

and 2). In addition, ranging and timing bias corrections have been determined along with the validation of mission orbit solutions. Ongoing application of the IRA methodology will be used to monitor ICESat instrumental biases and orbit and geolocation accuracy during the course of the mission.

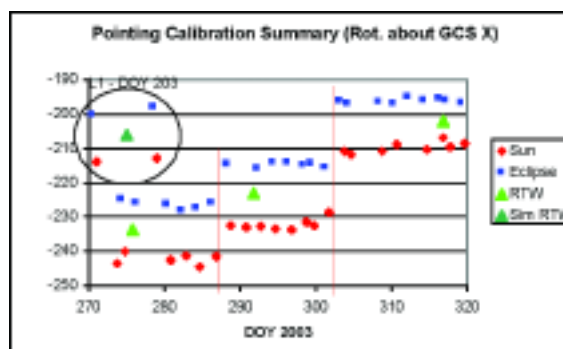


Figure 1. Laser 1 (L1 – circled and offset by 203 days) and Laser 2 (L2) pointing calibration summary. Each point on the graph represents the pointing calibration about the GLAS Coordinate System (GCS) X-axis from a single calibration maneuver. A distinct day/night orbital pointing variation is observed along with discrete jumps due to optical bench and laser temperature changes. The results show arc-second level calibration precision is being achieved.

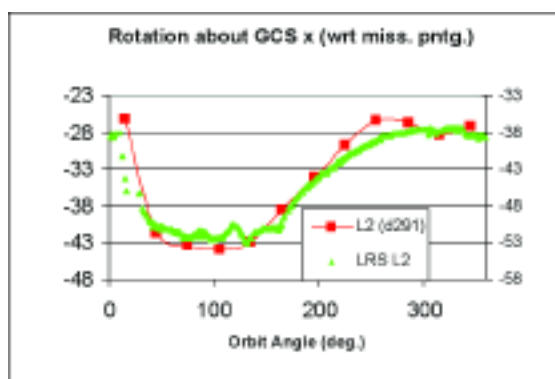


Figure 2. Results from a single calibration of the Laser 2 (L2) orbital variation in pointing. In this figure we compare our independent orbital pointing variation calibration determined from range residual analysis (red curve) with the orbital pointing variation observed by the GLAS Stellar Referencing System (SRS) instrument (green curve). The results show arc-second level agreement in the orbital variation about the GLAS Coordinate System X-axis is being achieved. In this comparison we have already calibrated the inherent bias in the SRS observations.

Contact: Scott B. Luthcke, Scott.B.Luthcke@nasa.gov

ICESat Calibration and Validation: Land Products

In addition to its primary objective of measuring ice sheet elevation change, the ICESat mission acquires globally distributed elevation profiles of the land surface. These profiles provide high-accuracy measurements of land and mountain glacier topography, tied to a uniform, global reference frame. They are useful for geodetic control of Digital Elevation Models and for observing topographic change caused, for example, by natural hazards and glacier dynamics. In addition, the backscatter waveforms acquired for each laser pulse characterize the within-footprint height distribution of illuminated surfaces, providing a means to measure geomorphic relief, due to ground slope and roughness, in vegetation-free areas and forest canopy height in areas of low relief.

The geolocation (horizontal and vertical position) and footprint surface parameters in the ICESat Land Products dataset are being validated by David Harding, Jeanne Sauber and Claudia Carabajal of the Laboratory for Terrestrial Physics. Techniques have been developed to assess geolocation accuracy by matching ICESat profiles to moderate resolution (10 to 30 m) Digital Elevation Models (DEMs) (Fig. 1) and by matching observed waveforms (Fig. 2) to simulated waveforms derived from high resolution (1 to 5 m) DEMs acquired by airborne lidar mapping of land and glacier cal/val sites.

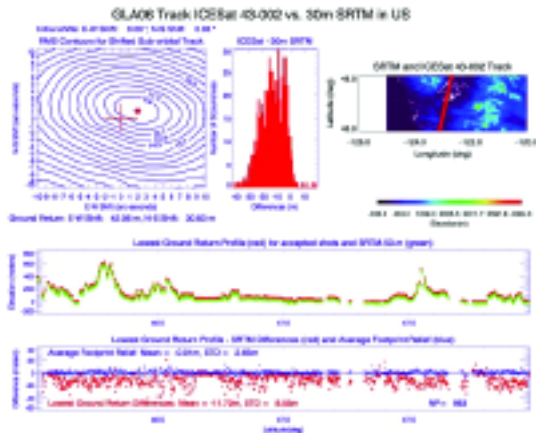


Figure 1. ICESat ground track (red) across color-coded Shuttle Radar Topography Mission DEM (top right), ICESat (red) and DEM (green, vertically offset for clarity) elevation profiles along the track (middle), elevation residual contours from profile shifting (top left) with starting location (plus) and best-fit location (asterisk), and elevation residuals (DEM minus lowest ground from ICESat waveforms) along the profile (red points, bottom) and as a histogram (top center).

Figure 1 shows a profile matching result, where iterative spatial searching defines the best-fit location based on minimization of profile-to-DEM elevation residuals, using a DEM from the Shuttle Radar Topography Mission (SRTM). This approach identified geolocation errors in initial ICESat data releases, and has confirmed improvements in subsequent releases that account for pointing biases. With the spatial match between ICESat and the DEM established, error characteristics of the DEM are quantified, such as the upward bias of the SRTM radar phase center elevations in vegetated areas.

Waveform matching provides a more precise assessment of geolocation accuracy and validates surface roughness and vegetation height parameters by utilizing very detailed DEM representations of ground or glacier topography and vegetation cover. A grid-based waveform simulation is used to approximate the laser pulse interaction with the Earth's surface using the high-resolution DEM as input and accounting for the ICESat pulse width and far-field energy pattern, and receiver FOV transmission and impulse response. Optimal matches are determined by minimizing the observed-to-simulated waveform residuals using an iterative spatial search. Observed to simulated waveform comparisons for forested landscapes (e.g., Figure 2) demonstrate that the ICESat waveforms are a very precise and accurate measure of the vertical structure of surfaces illuminated by the laser footprint.

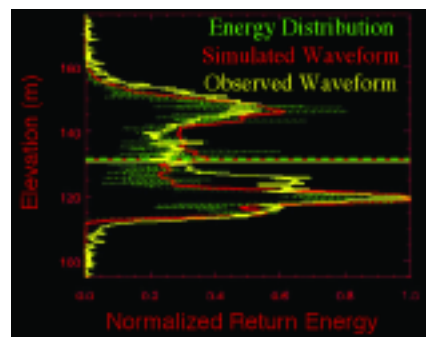


Figure 2. Elevation distribution of normalized energy for an observed ICESat waveform from a forested landscape (yellow) compared to the distribution of illuminated surfaces (green) and the resulting simulated waveform (red) at the ICESat footprint location obtained from a high-resolution DEM.

Contact: David Harding, David.J.Harding@nasa.gov

Precision Orbit Determination

Precise orbit determination (POD) is a major area of activity and expertise in the Space Geodesy Branch, Code 926. For some applications, as with satellite altimetry, POD enables science objectives such as the study of ocean, ice and land topography and surface change. In other applications, for example, reference frame and gravity field science is derived directly from the precise determination of orbits. In the year 2003 there has been a great deal of POD research activity within the Space Geodesy Branch. These activities have focused on analyzing Global Positioning System (GPS), Satellite Laser Ranging (SLR), Doppler Orbitography and Radiopositioning Integrated by Satellite (DORIS), and inter-satellite tracking data along with accelerometer, attitude and altimeter data. The analysis and research focuses on supporting the science objectives of several geodetic missions including: Jason-1, ICESat, GRACE, CHAMP, GFO, TOPEX/Poseidon and the geodetic laser ranging satellites along with interplanetary missions such as Mars Global Surveyor.

Members of the Branch develop and maintain NASA's state of the art precision orbit determination and geodetic parameter estimation system, GEODYN. The GEODYN system is capable of processing a myriad of Earth orbiting and interplanetary satellite tracking and altimeter (both radar and laser), accelerometer and attitude data for the purposes of altimeter science, reference frame and gravity research and development. The state of the art modeling and the ability to simultaneously process a wide spectrum of data types is a unique capability of the Branch. This capability was instrumental in our Jason-1 POD research, which achieved and validated the Jason-1 1-cm orbit accuracy goal, and characterized the remaining orbit errors and their impact on ocean topography research.

While there were many POD research activities in 2003, a major highlight was the achievement of the 1-cm radial orbit accuracy goal for Jason-1 (Luthcke et al. 2003). Achieving the Jason-1 1-cm radial orbit accuracy goal presented not only the challenge of producing these orbits, but also the challenge of demonstrating the accuracy of these orbits. The proper assessment of orbit accuracy, the determination of the best orbit strategy, and the characterization of the resultant orbit errors required the processing and analysis of multiple data types (GPS, SLR, DORIS, altimetry). We have demonstrated that our GPS-based reduced dynamic orbits achieve the 1-cm radial orbit accuracy goal and result in a significant improvement in the overall accuracy of the altimeter observations (Figure 1). We have also shown that a combination of GPS and SLR data produce orbits of higher accuracy than just GPS data alone. We have also developed models and orbit strategies that fur-

ther improve orbits computed without GPS data (using SLR, DORIS and altimetry). Further analysis of the altimetry using the new high accuracy GPS reduced dynamic orbits has revealed error and signal not previously observed, and has helped to characterize the stability of the altimeter data reference frame at the sub-cm level. The 1-cm orbit accuracy currently achieved for Jason-1 represents a significant improvement in radial orbit accuracy (2 cm was the standard for TOPEX/Poseidon) and will permit the resolution of new signals and features within the altimetry data.

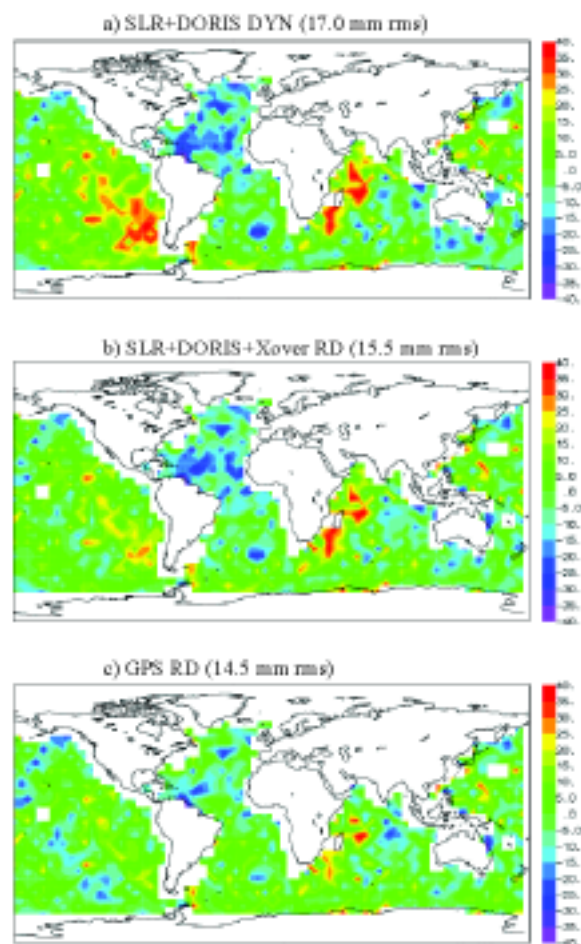


Figure 1. Crossover residuals averaged over 5°x5° bins for cycles 8-24 show radial orbit error primarily due to anti-correlated gravity error. The three maps show a progressive and significant reduction of this error from the dynamic SLR+DORIS to the reduced-dynamic GPS solutions. Crossovers offer an independent direct measure of orbit error, but also contain non-orbit signal.

For more details, see Luthcke, 2003.

Contact: David D. Rowlands, David.D.Rowlands@nasa.gov

Gravity models from CHAMP and GRACE

CHAMP and GRACE are the first in a series of new spacecraft missions to provide us with improved knowledge of the Earth's gravity field. CHAMP, launched in July 2000, is tracked by the global position system (GPS), and also includes a precision accelerometer to model non-conservative forces. The GRACE mission consists of two co-orbiting spacecraft with precise satellite-to-satellite tracking and ultra-precise accelerometers. The data from both spacecraft have dramatically improved our ability to model the Earth's geopotential. We have processed 87 days of CHAMP data in 2001 and merged these data with other precision tracking data from JASON, GFO, ENVISAT, STARLETTE, STELLA, and LAGEOS to produce a new CHAMP-era satellite-only geopotential model, GEM2003B (Goddard Earth Model 2003B). The CHAMP-only models significantly improve the high-degree modeling (Figure 1 and Table 1) and show notable changes over EGM96 in regions where the surface data (altimetry and surface gravity) were weak, such as over the high-latitude regions, the Amazon, the Himalayas and portions of Africa. The predicted gravity error with the CHAMP model is improved by nearly an order of magnitude at the lower degrees. However, geopotential models derived from CHAMP data alone do not properly model the resonances of certain key satellite orbits. It is for this reason that we have added data for certain important geodetic satellites in order to capture the resonances for these orbits.

Three days of Level-1B data were released to the GRACE science team and we have evaluated these data by adding them to the GEM2003B solution. We processed the satellite-to-satellite range data and accelerometry data for these days (April 25-27, 2003) and weighted the GRACE data in this test solution at $3.16 \mu/s$. Figure 2 illustrates the logarithm of the standard deviations for the geopotential solutions before and after adding the GRACE data. The improvement in the uncertainties is particularly dramatic in the band from degrees 40 to 80.

Model	
EGM96S	10.193
EGM96S + TDRSS satellites	8.746
GEM2003A, (CHAMP-only 87 days)	2.804
EIGEN3p (CHAMP-only, ~3 years)	1.183
GEM2003B	2.700
GEM2003B + 3 days of GRACE data	1.133
GGM01S (~111 days of GRACE data)	0.848

Table 1. Comparison of altimeter-derived anomalies. As an independent test, we compare the anomalies derived from the satellite-only geopotential models with those derived independently from satellite altimetry, and calcu-

late the variance of the anomaly differences through degree 70. This test shows that the models from CHAMP and GRACE are improved significantly over those containing the earlier generation of tracking data. The Eigen3p model (from GFZ/GRGS), and the GGM01S models (released by the GRACE project) are shown for comparison.

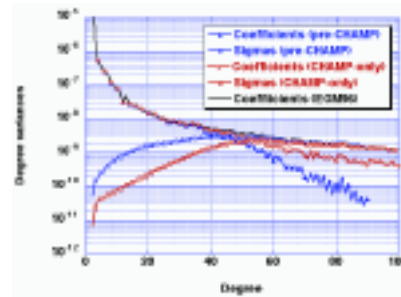


Figure 1: Degree variances for pre-CHAMP and CHAMP derived satellite-only geopotential models. The CHAMP data significantly enhance the power in the models at the higher degrees which cannot be sensed by the older generation of tracking data.

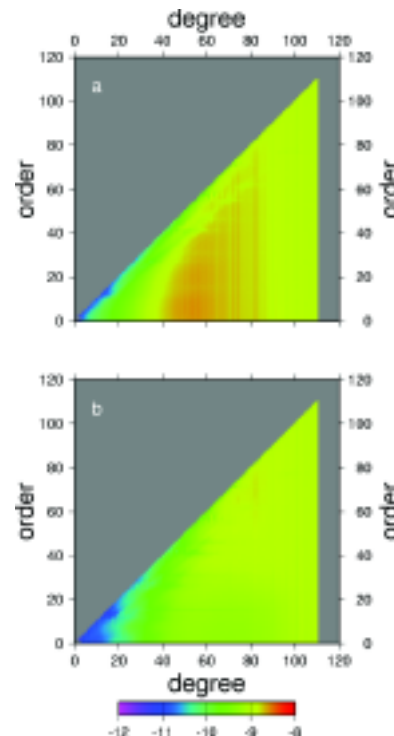


Figure 2. Logarithm of the standard deviations of the geopotential coefficients by spherical harmonic degree and order for (a) GEM2003B, (no GRACE data), and (b) GEM2003B + three days of GRACE data.

Contact: Frank G. Lemoine, Frank.G.Lemoine@nasa.gov

Satellites Seek Gravity Signals for Probing the Earth's Interior

For the past 4 decades, models of mantle convection have made remarkable advances. However, the global seismotectonic stresses in Earth's interior due to mantle convection are yet to be determined. The problem is that no one has been able to come up with a satisfactory scenario that characterizes the deformation stresses in Earth which can cause earthquakes and create tectonic features.

The fundamental problem of the deformation of the Earth involves stress conditions on the base of the crust caused by mantle convection. Convection-generated stresses can be inferred from satellite gravity models. The new gravitation model EGM96 has improved spherical harmonics of the model to degree and order of 360. In order to provide insights into the origin of earthquakes and prove the existence of the mesospheric plates which range in depth from 100 km to 300 km, Liu et al. (2003c) have developed a global stress pattern from satellite gravity models as shown in Fig.1, in which the length of the arrows represents the magnitude of the stress strength. Figure 1 seems to suggest a stress origin of shaping our world. Large earthquakes are shown to be restricted in the global belts of stress concentration. It is confirmed that the boundaries of the Hawaiian, Tristan and Icelandic mesoplates are subjected to large stress concentration.

Satellite detected stress concentrations are particularly intense in the ring of fire around the Pacific as indicated by strong convergence of arrows. These are the Western U.S., the Andes and the associated ocean trenches, off the Tonga and Japan trenches and near the East Indies. An important aspect of these stress belts relative to earthquakes is the implication for seismic hazard assessment. It has been found that the satellite detected stress belts around the Pacific and the statistically significant prediction of the Circum-Pacific seismic belts are in good

agreement. These research results indicate that the triggering stresses of the large earthquakes in the ring of fire around the Pacific and over the world could be detected by satellites.

The stress fields thus derived also have possible applications in earthquake prediction studies. The US/China joint earthquake prediction program beginning in 1981 has presented a thorough study of the relationship between gravity variations and seismotectonic stress changes under the Beijing-Tianjin-Tangshan-Zhangjiakou (BTZ) region in China. It has been proposed to seek gravity signals for probing seismotectonic stress changes under the BTZ region.

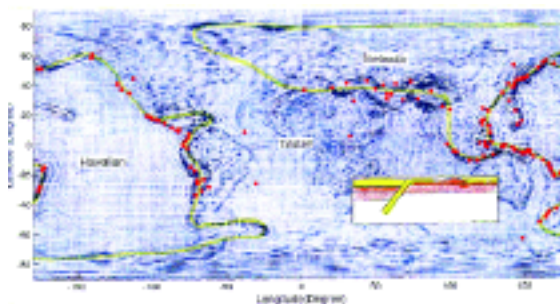


Figure 1. This equatorial equidistant seismotectonic stress map as inferred from satellite gravity signals up to the 150 harmonic degree shows approximate boundaries of the Hawaiian, Tristan and Icelandic mesoplates (200 km below Earth's surface). Formation of the three mesoplates has provided a framework for resolving a decades-old controversy (Pilger 2003) and explaining these destructive tectonic stresses as the origin of the 131 $M_s > 7.0$ earthquakes during 1977 to 2000. Inset: Cartoon section of lithoplates, asthenosphere and mesoplates.

Earth's Long-Wavelength Time-Variable Gravity Field and Geophysical/Climatic Causes

Cox and Chao [2002] reported in *Science* the detection of a large anomaly in the time series of Earth's dynamic oblateness J_2 , the lowest-degree gravity spatial harmonic, in the form of a positive "jump" that occurred in 1998. Continued analysis of Satellite Laser Ranging (SLR) data shows that J_2 has been rapidly returning toward "normal" since early 2001. Shown in Figure 1 is the observed non-seasonal J_2 time series, after removal of the pre 1998 linear trend associated primarily with post-glacial rebound, and the corresponding time series computed for the atmosphere. The departure between these series sometime in 1998 is evident.

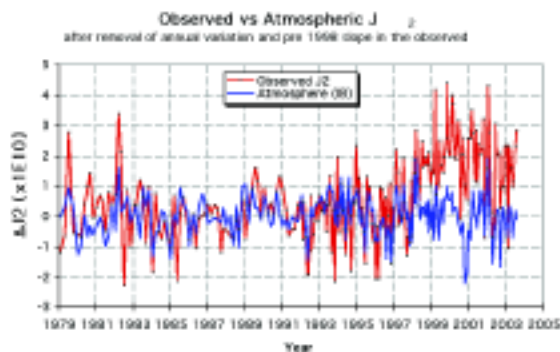


Figure 1. Comparison of non-seasonal J_2 between the atmosphere-induced and SLR-observed; note the departure around 1998.

An anomalous event took place in the extratropic Pacific Ocean at the beginning of 1998 and lasted several years until rapidly returning toward "normal" after 2001. This event has a remarkable correlation with the J_2 time series. (See Figure 2.) This time evolution is unequivocally captured in the leading Empirical Orthogonal Functions/Principal Component (EOP/PC) modes of sea-surface height data from TOPEX/Poseidon, sea surface temperature data from NCEP, and various parameters from the ECCO ocean circulation model including ocean bottom pressure (OBP), temperature, and salinity profiles. These effects appear to all be part of the manifestation of the Pacific Decadal Oscillation (PDO), thus having certain indirect link with ENSO, and general interannual climate changes.

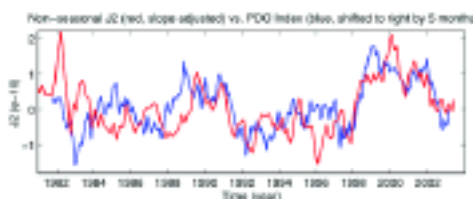


Figure 2. Comparison of the non-atmospheric interannual variation of the SLR-observed J_2 with the Pacific Decadal Oscillation Index.

The PDO time evolution matches remarkably well the 1998-2002 anomaly signature observed in the Earth J_2 series. However, the OBP field simulated by the ECCO ocean general circulation model predicts an anomaly in J_2 that is smaller by a factor of about 3 in magnitude than that observed. Some of the discrepancy is made up when changes in hydrology and glacier mass loss is considered. At this time, however, many questions remain open and the J_2 enigma continues. A complete resolution requires further in-depth studies exploiting various data types for the many related climatic phenomena.

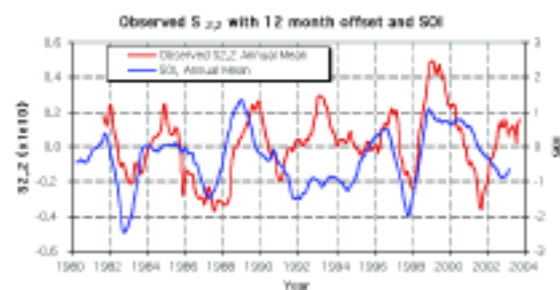


Figure 3. Comparison of interannual variation of the SLR-observed S_{22} component in the gravity field with the ENSO Index.

The SLR data can also be used to solve for various other low-degree harmonics. Figure 3 shows the smoothed signal extracted from the SLR-observed non-seasonal component of the $S_{2,2}$ gravity series. This spherical harmonic parameter describes the longitudinal distribution of mass within the Earth system. There is a correlation of 0.45 with a 12 month offset with the Tahiti-Darwin Southern Oscillation index (SOI), with the gravity signal preceding the SOI. The observed signal has too much power to be explained by the output of the ECCO ocean model. Comparison with NCEP-derived soil moisture series does explain some of the signal, especially for the 1997-98 El Niño.

This research exemplifies an interdisciplinary endeavor where geophysical observations made by space geodesy leads to insights about climatic phenomenon. The time-variable gravity integrates all mass changes in the entire Earth system. Sorting out the individual contributions requires reasonable spatial resolutions, which a single global quantity such as J_2 does not carry. Work is presently underway to extract more spatial resolution from the SLR dataset, and to combine the analysis with GRACE mission gravity data. These two data sets are complementary, especially given the limitations of GRACE in recovery of the very lowest degrees of the gravity field.

Contact: Ben Chao, Benjamin.F.Chao@nasa.gov

Earth System Center-of-Mass and Geophysical Fluids Transport

The center of mass of the Earth system is the point that "falls" towards the Sun in its solar system barycenter motion. It is also the well-known point defined by the standard Mechanic's laws. Satellites orbiting Earth "fall" towards that point, which defines the focus of their orbital trajectory. Using the tracking from earthbound stations, we can determine these trajectories and the locations of the tracking sites (coordinates) in a reference frame that has its origin very close to the terrestrial center of mass. The origin of this system is realized through the estimated coordinates of its defining set of positions and velocities at a chosen epoch, constituting the conventional Terrestrial Reference Frame (TRF).

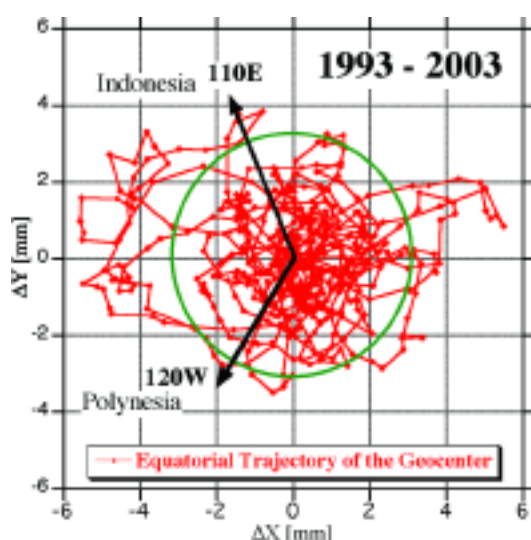


Figure 1. Equatorial trajectory of the geocenter for the 1993 – 2003 period. The 3-mm circle indicates the nominal motion, while the arrows indicate the geographical areas associated with excursions during El Niño /La Niña years.

For over three decades, these coordinates are determined through space geodetic techniques. The continuous redistribution of mass within the Earth system is the primary reason why the origin of this frame does not coincide exactly and at all times with the center of mass, the "geocenter." The geophysical fluid envelope of the planet, with its continuous redistribution of mass relative to the solid body of the planet (on which the tracking stations reside), continuously changes the position of the geocenter. The relocation of that point causes concomitant changes in the first-degree Stokes' coefficients describing the terrestrial gravity field, which is sensed by the satellites orbiting around Earth in trajectories governed by that field. Seasonal changes in these coefficients have been closely correlated with mass transfer in the atmosphere,

hydrosphere, and the oceans. The primary goal of the new gravity-mapping missions, CHAMP and GRACE, and the future mission GOCE, address these temporal changes from the gravimetric point of view. For the very low degree and order terms, there is also a geometric effect that manifests itself in ways that affect the origin and orientation between the instantaneous and the mean reference frame. To date, Satellite Laser Ranging (SLR) data from LAGEOS 1 and 2 contributed the most accurate results yet, demonstrating millimeter level accuracy for weekly averages of the location of the geocenter and daily averages of the orientation of Earth in the TRF. Analysis of over a decade of LAGEOS 1 and 2 SLR data at the JCET/GSFC Analysis Center for the International Laser Ranging Service produced one of the most uniform and accurate series of geocenter variations. The series revealed the indirect observation of geophysical events imprints on the geocenter motion. The axial component (z) is the dominant, driven by northern-southern hemisphere mass exchanges at annual and seasonal periods. A comparison of the equatorial trajectory of the geocenter with respect to the TRF (Fig. 1), revealed a strong correlation with two of the most recent El Niño / La Niña events. This correlation is understandably high since these events are associated primarily with mass transports in regions close to the equator. The interpretation of these observations and the comparison to oceanographic observations complements the existing observational record and provides an independent source for validation and better understanding of the underlying mechanism.

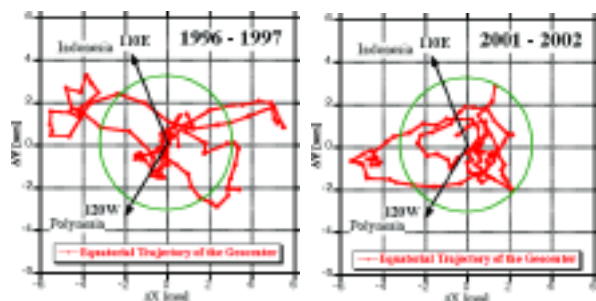


Figure 2. The two figures illustrate the departure of the geocenter from nominal motion during the two recent El Niño /La Niña events.

The 2-mm shifts in the geocenter can be explained as an increase in the mean sea surface height by an influx of roughly 2000 km³ of additional water spread over a cap of 50° radius and centered in the south Pacific basin. Based on the oceanographic observations of these two events, this is a very plausible explanation, given the fact that the total increase exceeds 30-40 cm for such events.

Contact: Erricos Pavlis, Erricos.C.Pavlis.1@gsfc.nasa.gov

Validation Study of Jason-1 Ocean Wave Heights

Over the past decade, satellite altimetry has been an indispensable tool for observing global ocean waves. Wave heights are determined from radar altimeter data by analyzing the returned waveforms: the steeper the leading edge of the returned waveform, the smaller the ocean wave. Altimeter data so collected are routinely used in numerical ocean-wave prediction programs, either for model tuning and validation or for direct data assimilation. Moreover, satellite altimetry is clearly the only mechanism for obtaining wave measurements of a global nature and over extended periods of time. Such measurements are beginning to be used in interesting studies of global and regional wave climatology as well as for many varied operational uses. For such applications it is critical that careful calibration and validation studies be performed. The work described here addresses this need for the new data being collected by the Jason-1 satellite altimeter, the successor mission to the successful Topex/Poseidon (T/P) mission. We have concentrated on the Jason-1 measurements of significant wave height, as well as some ancillary data such as radar backscatter cross-sections.

The verification phase of the Jason-1 mission provides a unique opportunity for such a study. For a period of about six months, from January through August 2002, the Jason and T/P satellites were flying in tandem formation along the same ground-track, separated in time by only 70 seconds. Such near-simultaneous measurements allow these two systems to be compared and calibrated against one another in an unprecedented manner. Our study also used independent wave-height data collected at 20 moored deep-sea buoys and wave-height predictions from a NOAA numerical operational wave model (WaveWatch-III).

In summary, the Jason wave-height data are found to be of high quality, surpassing the original mission precision specifications, although the data are slightly noisier than Topex data and appear to be slightly smaller than Topex heights. This is easily seen in the satellites' joint distribution diagram, shown in Figure 1. A fit to the data of this figure yields a slope of 1.030, for a 3% difference on average. (This result is based on an orthogonal regression analysis, which accounts for errors in both systems.) The subtle bowing of contours in Fig. 1 near Jason 4-meter waves is caused by additional noise in the Jason measurements. The RMS difference between the two system measurements is 28 cm, and this can be reduced by nearly half by some improved outlier-detection and smoothing methods.

For details, see Ray and Beckley, 2003.

Contact: Richard D. Ray, Richard.Ray@nasa.gov

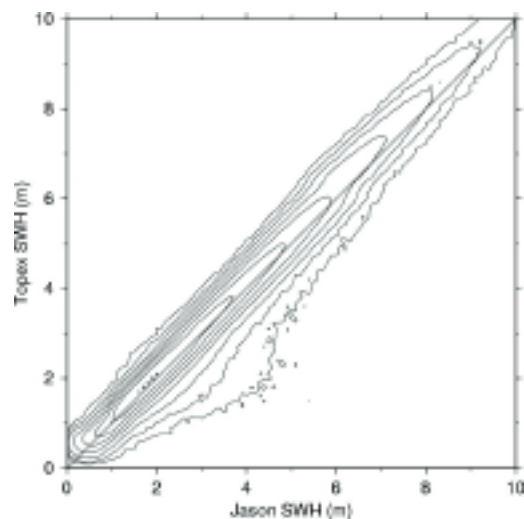


Figure 1. Observed joint probability density function of near-simultaneous Jason and Topex Significant Wave Height measurements, collected over a 6-month period. Contours are roughly logarithmic, from 0.0003 to 1 m⁻². The slope of the main bulk of data slightly exceeds unity, indicating that Jason is returning wave heights slightly smaller than Topex's.

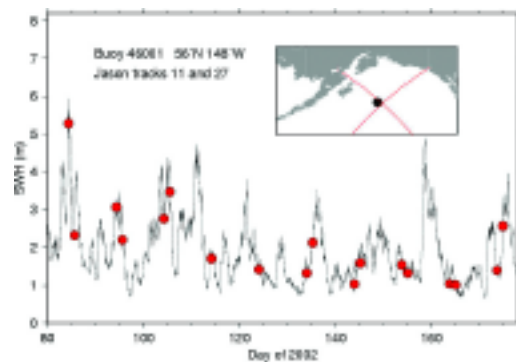


Figure 2. Comparison of Jason-1 measurements of the ocean's Significant Wave Height (red circles) along two ground-tracks over the Gulf of Alaska. The tracks pass near NOAA Buoy 46001 which has collected a continuous time series of wave heights (black line). Jason flies over each ground-track once every 10 days. An analysis of 20 such time series gives an RMS difference between Jason and buoy measurements of 21 cm.

Atmospheric Rotational Effects on Mars Based on the NASA Ames General Circulation Model: Angular Momentum Approach

The objective of this investigation is to use the angular momentum methodology to compute and analyze how the atmosphere affects the equatorial components of the rotation of Mars, based on outputs from the NASA Ames General Circulation Model (GCM). The model provides values of wind velocity, density and pressure, which serve as inputs to the calculation of the terms which appear in Liouville's equations.

The rotational variations of a planet can be analyzed into axial and equatorial components. The axial variations (along the z-axis, which is the rotation axis) are reflected in changes in the length of day (LOD). The equatorial variations (x, y) produce changes in the orientation of the axis of rotation (polar motion). The solution of Liouville's equations provides the changes in planetary rotation, i.e., changes in LOD and polar motion.

The methodology of planetary rotational investigations can follow the angular momentum approach or the torque approach. The chosen methodology determines the boundaries of the appropriate control volume. The angular momentum method involves the computation of terms containing the products of inertia of the atmosphere ("mass terms") and their time derivatives, as well as relative angular momentum terms ("motion terms") and their derivatives.

The torque approach was used by us in a previous investigation to compute polar motion and LOD variations. The LOD variations were computed also using the angular momentum methodology.

The NASA Ames GCM is a finite difference model based on the primitive equations of meteorology expressed in spherical sigma coordinates (σ = pressure at height / surface pressure). The resolution is 7.5° (latitudinal) by 9° (longitudinal). The version of the model used here has 30 vertical layers extending from the surface to 100 km. The output files are written every 1.5 hours of simulated time, 16 times per sol. There are 10704 records in the data file, representing a time span of 669 sols (687 Earth days) which is the length of the Martian year.

The outputs from the NASA Ames GCM provide a 1.5 hour sampling rate. Therefore the results for the forcing functions are not limited to annual and semi-annual components.

The condensation and sublimation of CO_2 on the surface and

in the atmosphere of Mars produce changes in the atmospheric mass distribution as well as changes in the polar caps. From the standpoint of rotational dynamics these changes are manifested in time variations in the moments and products of inertia. Another source of rotational variations is due to the atmospheric winds, which contribute to the relative angular momentum terms.

The amount of atmospheric mass involved in condensation and sublimation is equal to 16.52% of the total atmospheric mass.

It is possible to consider the (x, y) components of the polar displacement as components of a vector characterized by magnitude = $(x^2 + y^2)^{1/2}$. The maximum pole displacement due to ice formation and sublimation is 32.8 cm, occurring at 548 sols. Atmospheric mass variations yield a maximum of 40.9 cm at 478 sols. The combined effect has a maximum of 35.3 cm at 616 sols.

Table 1 lists the main harmonics for the solution combining the ice caps and atmospheric mass variation effects. The amplitudes of the (1/4)-annual and (1/3)-annual harmonics for the combined solution are certainly within the range of detection of future geodetic missions to Mars, such as the planned NetLander Ionospheric and Geodesic Experiment (NEIGE).

Table 1. Main harmonics of polar motion displacement: $\sqrt{x^2 + y^2}$. Ice and atmospheric effects combined.

Cycles per year	Period (sols)	Amplitude
4	167.25	3.96
3	223	3.03
1	669	2.52
2	334.5	0.79
5	133.8	0.61
8	83.625	0.58
9	74.333	0.45
6	111.5	0.43
13	51.4615	0.33
7	95.5714	0.32

Polar Wander on Triton and Pluto

Polar wander may occur on Triton and Pluto because of volatile migration. Triton, with its low obliquity (obliquity is the tilt of the axis), can theoretically sublime volatiles (mostly nitrogen) at the rate of $\sim 10^{14}$ kg yr⁻¹ from the equatorial regions and deposit them at the poles. Assuming Triton to be rigid on the sublimation timescale, after $\sim 10^5$ years the polar caps would become large enough to cancel the rotational flattening, with a total mass equivalent to a global layer ~ 120 -250 m in depth. At this point the moon overbalances and the pole wanders about the tidal bulge axis, which is the line joining Triton and Neptune (see Figure 1). Rotation about the bulge axis might be expected to disturb the leading side/trailing side cratering statistics; the leading side bashes into more meteorites and asteroids. Because no such disturbance is observed, it may be that Triton is too stiff or its surface volatile inventory too low to permit wander.

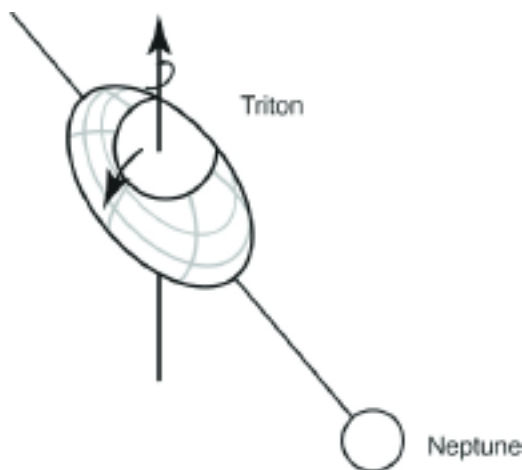


Figure 1. High Viscosity Wander

On the other hand, its stiffness might be low, so that any size cap might be expected to wander toward the tidal bulge axis (see Figure 2). In this case, the axis of wander passes through

the equator from the leading side to the trailing side; rotation about this wander axis would not disturb the cratering statistics. Polar wander may explain the bright southern hemisphere: this is the pole which is wandering toward the equator, while the other hemisphere tilts out of view. In any case the "permanent" polar caps may be geologically very young. Polar wander may also take place on Pluto, due to its obliquity oscillations and perihelion-pole geometry. However, Pluto is probably not experiencing any wander at present. The Sun has been shining strongly on the poles over the last million years, so that volatiles migrate to the equator, stabilizing the planet against wander. Spacecraft missions to Triton and Pluto which measure how flat the objects are could give information about the accumulation of volatiles at the poles. Such information is best obtained by measuring gravity and topography from orbiters, as was done for Mars with the highly successful Mars Global Surveyor.

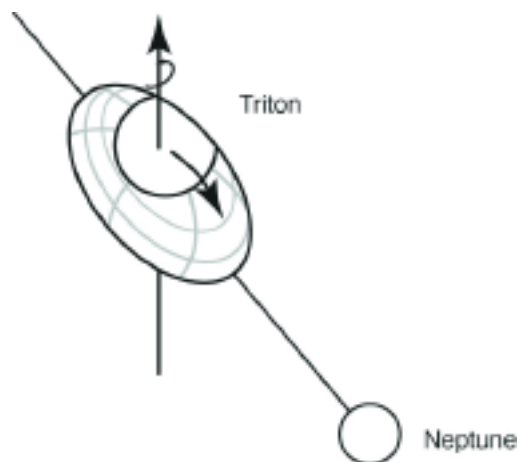


Figure 2. Low Viscosity Wander

For more details see Rubincam, 2003.

A Solar System Survey of Forced Librations in Longitude

Forced librations in longitude are periodic variations in the spin rate of a planetary body arising from gravitational interactions with an orbital partner. The analytic theory we have developed allows us to examine expected amplitudes of forced librations for bodies occupying a wide range of spin states: non-resonant, non-synchronous but resonant (e.g. Mercury), and synchronous. The theory has been applied to 33 solar system bodies including the planets, many planetary satellites, and Eros.

This study has been motivated by the recognition that the rotational response of a planetary body to external gravitational perturbations can be used to probe its internal density structure. Thus observations of forced libration amplitudes can provide a method for a remote determination of a body's radial mass distribution. Comparison of such observations with our calculated libration amplitudes (where we have assumed a uniform density, rigid body) should allow for discrimination of complex, radial density distributions from simpler, near homogeneous cases. The phase and amplitude of librations for a body with density stratifications will be much different than those exhibited by a homogeneous, rigid body. Calculations of expected librations can supply amplitude estimates helpful in determining whether librational dissipation may be important, and in identifying the likelihood of detecting librations observationally.

Our approach makes several simplifications. While a rotating body in the presence of a gravitational partner will exhibit changes both in spin rate, and spin direction if the orbit-normal and spin vector are not parallel, we assume zero obliquity so that gravitational torques excite only changes in spin rate. This method will not be as accurate for bodies with large obliquities, such as Earth. The time scale over which forced librations operate are sufficiently short compared to the time scale for orbital evolution that we assume fixed Keplerian ellipses for the orbits.

Librational amplitude estimates are derived by expressing the behavior of the system as a balance between external torques, and the response of the body. We write the torque as a function of several parameters: the body's departure from spherical symmetry, expressed as the moment difference

$$\sigma = \frac{B - A}{C},$$

the angular orientation θ of its principal axis a , measured from an inertially fixed reference direction; and the body's orbital

position expressed as true anomaly f , which is angular distance from periape. In terms of those parameters, we write the rotational response to the torque as

$$\frac{d^2\theta}{dt^2} = -\frac{3\sigma n^2}{2} \left(\frac{a}{r}\right)^3 \sin[2(\theta - f)].$$

If we assume that the unperturbed state of the body is steady rotation, then the angle can be decomposed into a steady component pM , and a small libration angle γ , where p is the ratio of the body's rotation rate to its orbit rate, and M is mean anomaly. We then expand orbital position as a Fourier series in eccentricity (e), and mean anomaly (M), resulting in a Fourier-like series representation of the forcing that is periodic in time.

The librational response γ will take the same form as the forcing, and equating coefficients between the expected form of γ and the series expansion for the forcing yields the series solution for forced librations

$$\gamma = \frac{3\sigma}{4} \sum_{q=0}^{\infty} F_q^+ + F_q^-$$

with

$$F_q^+ = \frac{C_q^{-3,2} - S_q^{-3,2}}{(2p+q)^2} \sin[(2p+q)mt]$$

$$F_q^- = \frac{C_q^{-3,2} + S_q^{-3,2}}{(2p-q)^2} \sin[(2p-q)mt]$$

where C_q and S_q are Cayley coefficients.

Application of this series solution to solar system bodies shows that the dominant libration amplitude always occurs at frequency $2(p-1)n$ or semi-diurnally as seen from a reference frame centered on the torquing primary. For a rigid body, the angular amplitude for the forced librations of a synchronous rotator can be approximated as

$$\gamma = 6 \sigma \epsilon$$

and for a rigid, non-synchronous rotator, the libration angular amplitude can be estimated by

$$\gamma = \frac{3}{16} \frac{2 - 5e^2}{(p-1)^2} \sigma.$$

Contact: Bruce Bills, Bruce.G.Bills@nasa.gov

The Role of CO₂ in Orbital-Scale Climate Changes

Correlation analysis can be applied to climate-related time series for investigating the causal relationship between CO₂ concentration and climate change. A new analysis by Liu, Kolenkiewicz and Wade (2003a), has shown that fluctuations in insolation reaching the Earth due to orbital and rotational motion of the solid Earth can explain major climate changes up to recent time and that the sensitivity of climate to the concentration of CO₂ is much less than previously estimated. The new study shows that insolation pulsation in terms of surplus of solar heating due to orbital motion is associated with the climate changes and atmospheric concentrations of CO₂.

Ice cores provide access to palaeoclimate data series that include local temperature and precipitation rate, moisture source conditions, wind strength and aerosol fluxes of marine, volcanic, terrestrial, cosmogenic and anthropogenic origin. They are unique with their entrapped air inclusions in providing direct records of past changes in atmospheric trace-gas composition. The ice drilling project has already provided a wealth of such information for the past three glacial-interglacial cycles. In particular, there is a close and strong correlation between temperature variations and atmospheric concentration of CO₂. This discovery may argue that CO₂ is important as amplifier of the initial orbital forcing and may have significantly contributed to the abrupt climate changes. But this does not mean that CO₂ concentration is the cause of glacial-interglacial climate change. In fact, CO₂ concentrations during the past 350 thousand years are the effect and consequence of rapid temperature increases caused by insolation pulsation. Therefore, ice core results should not be used to infer an empirical estimate of the sensitivity of global climate to future anthropogenic increases of CO₂ concentration.

In addition, the new study has found that the intensity of the insolation pulsation is dependent on latitude. At high latitude, it provides extreme climate warming conditions for green-

house-gas concentration. However, the climate warming effect decreases markedly in low latitude regions, predicting cool tropical temperature during supposed greenhouse episodes. It appears that this is what is recently recorded in the ice drilling project. Therefore, the new research development of insolation pulsation may provide an important physical mechanism for understanding the cool-tropic paradox in the current climate models of global greenhouse warming. Only the insolation pulse can stimulate an extraordinarily efficient heat-transport mechanism on Earth.

Much of the current debate on climate change is driven by the observation of anthropogenic CO₂ concentration. Global greenhouse warming is controversial because the primary role of CO₂ in determining global temperature is in question. This study is of relevance with respect to the continuing debate on climate change in the future.

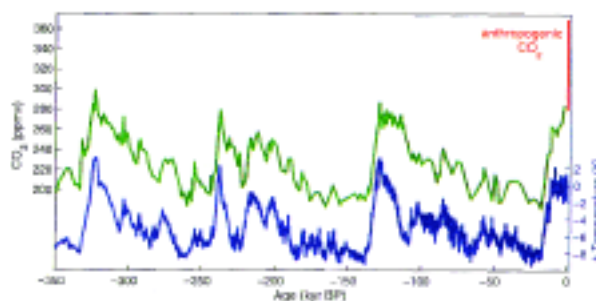


Figure 1. Fluctuations of temperature (blue) and CO₂ (green) for the past 350 kyr from the Vostok ice core records. The recent anthropogenic rise in CO₂ is marked in red.

For details see Liu et al., 2003a.

Gravitational Core-Mantle Coupling and Length-of-day

The tides are slowing down the rotation of the Earth, overwhelming a smaller positive acceleration from postglacial rebound. According to historical records such as ancient and medieval observations of solar eclipses, the signal from these two secular effects appears to be significantly corrupted by a source (or sources) of an episodic or perhaps periodic nature operating on a 1000 year timescale. This non-secular source causes accelerations which are the same order-of-magnitude as the tides, $\sim 6 \times 10^{-22} \text{ s}^{-2}$. Coupling between the liquid outer core of the Earth and the mantle has long been a suspected reason for changes in the length-of-day. Research heretofore has been aimed at viscous, electromagnetic, and topographic coupling at the core-mantle boundary, mostly on the decadal timescale, and at gravitational coupling not related to the problem treated here.

The present investigation focuses on the gravitational coupling between the density anomalies in the convecting liquid outer core and those in the mantle and crust as a possible cause for the observed non-secular acceleration on the millennial timescale. (Hereafter "mantle" is used as a shorthand for "mantle and crust.") The basic idea is as follows; there are density inhomogeneities caused by blobs circulating in the outer core like the blobs in a lava lamp; thus the outer core's gravitational field is not featureless. Moreover, these blobs will form and dissipate somewhat randomly. Thus there will be a time variability to the field. These density inhomogeneities will gravitationally attract the density anomalies in the mantle.

The outer core and mantle may not be in a state of gravitational equilibrium if the blobs form and dissipate faster than either the outer core or mantle can react to achieve a state of zero torque. In other words, the mantle and outer core may always be in a state of disequilibrium due to the stochastic nature of "core weather." The outer core and mantle will try to align with each other to make the torque between them zero; but before this can happen, the gravitational field of the outer core may change, so that the core and mantle never

catch up with each other. Hence it may be that the outer core is forever torquing the mantle, changing its rotation state and perhaps producing the observed non-secular acceleration and changing the length-of-day. By action-reaction the outer core will also change its rotation state.

A quantitative calculation indicates that the gravitational torque on the mantle from the liquid core may be sufficient to explain the accelerations and decelerations in the Earth's rotation on the 1000 year timescale. The corresponding torque by the mantle on the core may also explain the westward drift of the magnetic field of 0.2° per year. Gravitational core-mantle coupling would stochastically affect the rate of change of the Earth's tilt by just a few percent. Its contribution to polar wander would only be about 0.5% of the presently observed rate of 10 centimeters per year.

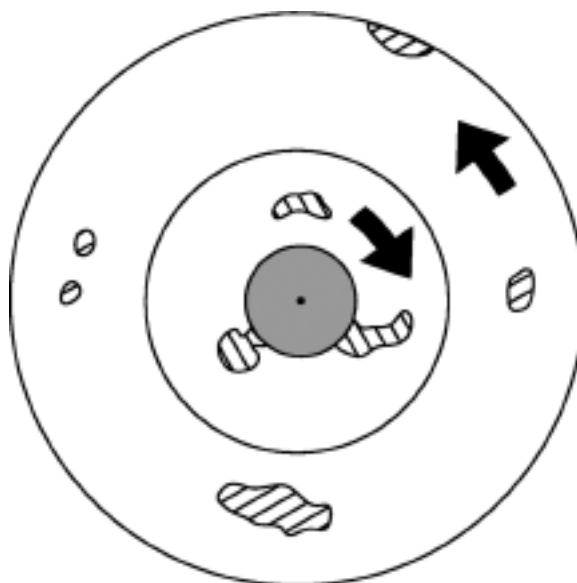


Figure 1. Blobs in the liquid outer core attract density inhomogeneities in the mantle, torquing the mantle.

For details, see Rubincam, 2003.

Geomagnetic Probing of Core Geodynamics

As Earth's magnetic field weakens, our magnetic shield against the onslaught of the solar wind thins. The field strength needed to fend off the magnetized solar plasma is decreasing, just as the delicate complexity of our vulnerable electro-technical systems is increasing at unprecedented rates. A working group of distinguished scientists from across the nation has asked NASA's Solid Earth and Natural Hazards program a key question: What are the dynamics of Earth's magnetic field and its interactions with the Earth system?

Some answers to part of this question come from studies of the core geodynamo, a dynamical system as complicated as weather and climate, yet buried deep beneath 1800 miles of rocky mantle. Electric current flowing in Earth's metallic core is the main source of the main field, but it is weakening faster than expected from the small electrical resistivity of the metal. According to one theory, as Earth cools over geologic time, the solid iron inner core freezes from the molten outer core. This liberates latent heat and buoyant slag which rise, stirring the outer core to motion at speeds of several miles per year. Whatever causes core fluid motion, dynamo action transforms kinetic energy of the motion into magnetic energy of the field. Some of this energy emerges as our largely dipolar magnetic shield. But sometimes the transformation may go the other way, with the core running like a motor instead of a generator. This may accelerate core motions, weaken our shield, and perhaps drive the main axial dipole field to zero and beyond - to reversed polarity.

Paleomagnetic studies of crustal rocks magnetized in the geologic past reveal that polarity reversals have occurred many times during Earth's history. Computer simulations of core field & flow, including effects of gravitational, pressure, Coriolis, magnetic and viscous forces, suggest how this might happen in detail. And space-based measurements of the real, time-varying magnetic field help constrain estimates of the speed and direction of fluid flow by the top of Earth's core.

Core flow estimates often omit small scale features, less than about 600 miles across, which are not easily resolved from

observed, broad scale changes in the field. Some estimates also neglect magnetic forces by the top of the core compared with other forces. Of course, when it comes to the scale of the flow and the strength of magnetic forces in a liquid metal hidden by 1800 miles of rock, doubts abound.

We have developed and applied methods to test both the hypothesis of narrow scale flow, and that of a dynamically weak magnetic field, by the top of Earth's core. Using two completely different methods, we have shown these hypotheses lead to a specific theoretical form for the spectrum of Earth's main magnetic field and a different form for the spectrum of its rate of change. Much as a prism separates light into its spectrum, from long wavelength red to short wavelength blue light, geophysicists use the digital prism of spherical harmonic analysis to separate the magnetic field into its spectrum, from long to short wavelength fields. And we do this for the rate of change of the field as well.

To test a hypothesis, the implied theoretical spectrum is fitted to an observational spectrum. This yields an estimate of the radius of Earth's core and its uncertainty. If the estimate agrees with the established value, determined by independent seismological techniques, then the hypothesis passes the test. The weak field and the narrow scale flow hypotheses each pass key tests, both separately and together. Recent analysis of data from the Danish Geomagnetic Research Satellite Ørsted, however, suggests the core flow may have become broader in scale, or better organized, in just the past 20 years.

For further information, including how compact eddies in a fluid conductor cause magnetic field changes over all scales, and how the magneto-geostrophic vorticity balance constrains kinetic-to-magnetic energy conversion atop the core geodynamo, see the paper, "Narrow scale flow and a weak field by the top of Earth's core: evidence from Ørsted, Magsat, and secular variation" by Coerte V. Voorhies, to appear in the American Geophysical Union's Journal of Geophysical Research - Solid Earth.

MoSST Core Dynamics Model: Applications to Surface Geodynamic Observables

This is part of our long-term research effort on modeling dynamical processes in the Earth's fluid outer core, interactions between the outer core and solid mantle, and applications of the model to other geodynamic/geodetic research. The central piece of our research tools is a Modular, Scalable, Self-consistent, Three-dimensional (MoSST) core dynamics model. The structure of this model is very flexible, such that any geophysical research/application can be added to this model as a component (module).

The Earth's fluid outer core is in vigorous convection through much of the Earth's history, driven by gravitational energy released through secular cooling of the Earth. This results in many geomagnetic/geodynamic phenomena observable at the Earth's surface. One group of geodynamic effects arises from the core fluid density variation on various spatial and temporal scales, i.e. large-scale mass redistribution in the core via convective flow. Two of them are of particular interest: time-variable gravity and gravitational coupling between the fluid outer core and the heterogeneous mantle. The latter can be important to explain Earth's rotation variation on decadal time scales. Understanding these phenomena helps not only explaining surface geodynamic observations, but also identifying possible observational evidences and constraints on dynamical processes in the fluid outer core, and thus on numerical model improvement.

One result from this research activity is that the gravity anomaly arising from mass redistribution possesses unique spatial-temporal patterns. Figure 1 is a time sequence of the gravity anomaly at the Earth's surface due to core mass redistribution. One can observe from the sequence that the time variable gravity is dominantly by low order spherical harmonic patterns, partly due to spatial filtering across the mantle. One could also observe from the figure that the gravity anomalies at the Earth's surface drift westward, similar to the magnetic field from numerical modeling. This research also suggests that the magnitude of the gravity anomaly (relative to the mean gravity) at the Earth's surface can be sufficiently strong ($\sim 10^{-11}$ /year), to be observable via space geodesy techniques, e.g. GRACE and GRACE follow-on missions.

With the presence of the mantle density heterogeneity (which can be derived from seismic observations), core density anomaly also results in gravitational interaction between the outer core and the solid mantle. This research shows that the coupling torque arising from the gravitational core-mantle interaction is stronger than that from electromagnetic core-mantle interaction.

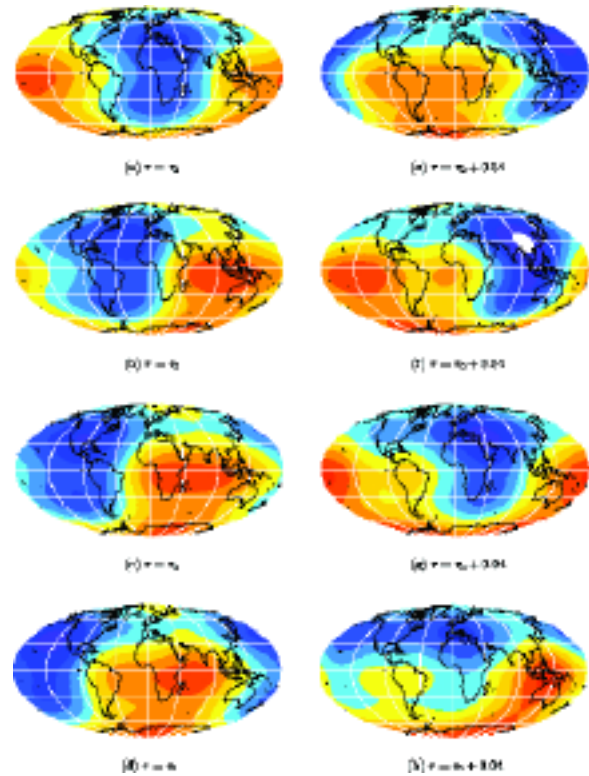


Figure 1: The gravity anomaly at the Earth's surface due to mass redistribution in the fluid outer core. The simulation time increases from top to bottom, and from left to right, with the increment $\delta t = 0.005$ (numerical time). The orange and blue colors represent the positive and the negative anomalies, respectively.

For detail, see Kuang and Chao 2003, and Kuang, 2003.

Obliquity, Precession, and Geomagnetism

The environment of the Earth is surrounded by a magnetic field which is believed to originate in the flow of the Earth's fluid core. Although specific heat sources in the Earth's core may produce convective motions which drive the dynamo, the dynamo process in the core which causes fluctuations of the geomagnetic intensity is a scientific mystery. Recently, geophysicists have integrated 33 records of geomagnetic intensity into a composite curve spanning the last 800 kyr (Sint-800). They have shown that the Earth's magnetic intensity fluctuated on a variety of time scales. The periods of their geomagnetic intensity fluctuations are almost identical with that of the precession modulation of the obliquity as obtained by Liu et al. (2003b). This suggests that the orbital-rotational coupling effect on the convection of the Earth's liquid core may be the geodynamo that generates the planet's magnetic intensity fluctuations.

In order to understand the Earth's orbital and rotational motion as the cause of geomagnetism, it is necessary to introduce some fundamental notions of celestial mechanics. Recent advances in celestial mechanics have led to precise results of precession modulation in the frequency of the Earth's obliquity, which is a crucial orbital parameter associated with the regeneration of the geodynamo. The frequency spectrum of the Earth's obliquity is shown in Fig. (a). It is calculated using gravitational attractions of the Moon, planets and Sun on the equatorial bulge of the Earth. The power spectrum, which peaks at 250-, 100-, 50-, 41-, 32-, and 26-kyr, may have physical implications with regard to intensity changes in the geomagnetic field.

Recent advances in geomagnetic dating techniques have led to precise records of the relative intensity of geomagnetism at numerous field sites. The spectrum of the Sint 800 record is shown in Fig. (b). It shows that the power spectrum peaks at 250-, 100-, 50-, 41-, 30-, and 26-kyr, which seems to mimic the frequency spectrum of the obliquity in Fig. (a). Therefore, the most important feature which the orbital imprint may be recognized in geomagnetic records is probably the precession modulation of the Earth's obliquity.

There is almost certainly significant convection in the outer core of the Earth, involving considerable energy transfer. This study shows that an external orbital effect could steer the form of the time variation of the geodynamo. The clear and strong correlation between the two spectra in Figures (a) and (b) seems to suggest that precession modulation of the obliquity frequency may be the primary power source which injects significant energy into the core to power the dynamo and dominates over direct thermal effect.

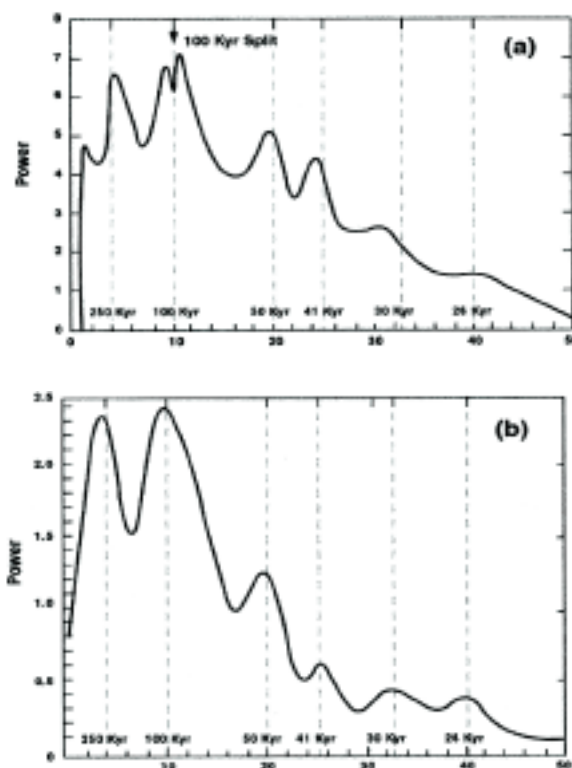


Figure 1. Power spectra are almost identical: (a) obliquity modulation spectrum of the precession over the past 800 kyr. (b) Virtual axial dipole moment (VADM) spectrum over the past 800 kyr (Sint 800).

Satellite-Altitude Magnetic Data over the Mineralized Region of Kiruna, Sweden

Satellite altitude (400 km) and aeromagnetic anomaly data have been analyzed over the Kiruna, Sweden iron mining district. The purpose of this investigation was to determine the relationship between large magnetic anomalies observed at satellite altitude and known mineral deposits. A nearly circular, well-defined Magsat magnetic anomaly (>9 nT) lies over this well-known iron-mining district. Aeromagnetic data were continued upwards to satellite altitude in order to compare them with the Magsat map. Figure 1 shows these data at 400 km altitude is shown in Figure 2.

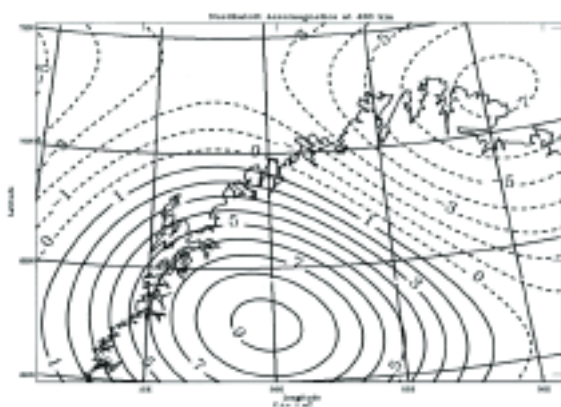


Figure 1. Nordkalott aeromagnetic data upward continued to 400 km altitude. Contour interval 1 nT with solid contour lines representing positive values, dashed the negative and zero contour.

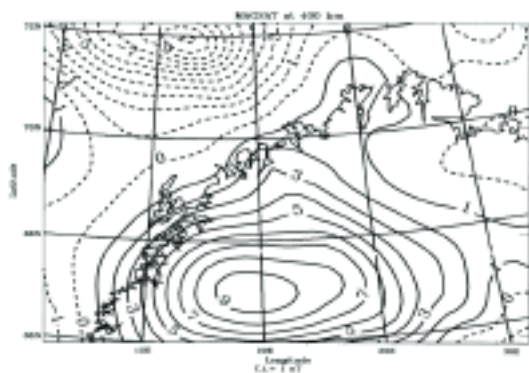


Figure 2. Magsat magnetic anomaly map computed at 400 km altitude. Contour interval 1 nT with solid contour lines representing positive values, dashed the negative and zero contour.

It is particularly noteworthy that the positive magnetic anomalies in both the satellite and upward continued aeromagnetic data are coincident and have the same value indicating that both data sets have the same zero-reference level. We can interpret this agreement to indicate that these two data sets are sensing the same anomalous magnetized body.

A map of the major fracture zone of this region (Billstrom et al., 1997) was superimposed on the Magsat anomaly map (Figure 3).

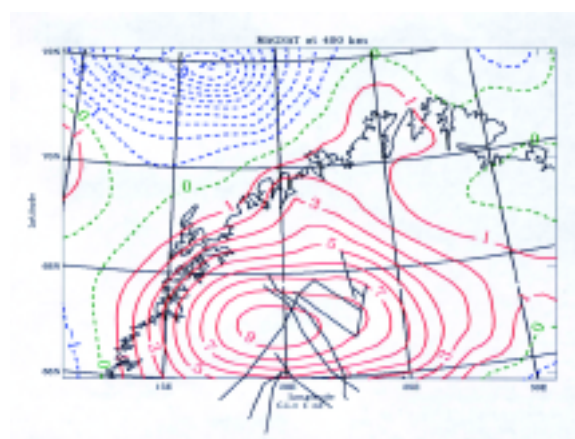


Figure 3. Figure 2 with fracture pattern superimposed.

The intersection of the major fracture zones lies slightly to the northeast of the Magsat anomaly center. It is, therefore, interesting to speculate that the anomalous magnetic mass causing the satellite-altitude anomaly is deep-seated and related to the fracture zone pattern. It has been proposed that major lineaments played a role in the emplacement of the ore deposits of Northern Sweden. The fracture zones could provide migration routes allowing this lower crustal material to be emplaced in the upper crust. We propose a relationship between this fracture pattern, the highly magnetic anomalous mass causing the satellite altitude magnetic signature and the iron ore body with the fracture pattern localizing the mineralization.

For detail, see Taylor and Frawley, 2003.

Refereed Publications

- Chao, B. F.**, Geodesy is not just for static measurements any more, EOS, Trans. Amer. Geophys. Union, 84, 145-156, 2003.
- Cohen, S.C.** and D.J. Darby, Tectonic plate coupling and elastic thickness derived from the inversion of geodetic data using a steady-state viscoelastic model: Application to southern North Island, New Zealand, J. Geophys. Res., 108(B3), 10.1029/2001JB01687, 2003.
- Comstock, R.L., and **B.G. Bills**, A solar system survey of forced librations in longitude, J. Geophys. Res. Planets, 108, 5100, 2003.
- Duncan, C., **J. Masek**, and E. Fielding, How steep are the Himalaya? Characteristics and implications of along-strike topographic variations, Geology, 31 (1): 75-78, 2003.
- Egbert, G. D. and **R. D. Ray**, Semi-diurnal and diurnal tidal dissipation from Topex/Poseidon altimetry, Geophysical Research Letters, 30(17), 1907, 2003.
- Egbert, G. D. and **R. D. Ray**, Deviation of long period tides from equilibrium: kinematics and geostrophy, Journal of Physical Oceanography, 33, 822-839, 2003.
- Fomalont, E., **L. Petrov, D. S. McMillan, D. Gordon**, and **C. Ma**, The second VLBA calibrator survey - VCS2, Astronomical Journal, 126 (N5), 2562-2566, 2003.
- Haugerud, R., **D.J. Harding**, S.Y. Johnson, J.L. Harless, C.S. Weaver, and B.L. Sherrod, High-resolution topography of the Puget Lowland, Washington - A bonanza for earth science, GSA Today, 13(6): 4 – 10, 2003.
- Heirtzler, J. R.** and K. Nazarova, Geomagnetic secular variation in the Indian Ocean, Earth Planet. Sc. Lett., 207 (1-4): 151-158, February, 2003.
- Kuang, W. and B.F. Chao**, Geodynamo modeling and core-mantle interactions, Geodynamics Series, 31 (eds. Dehant, Creager, Karato, Zatman, AGU Monograph, AGU, Washington, DC), 193-212, 2003.
- Kuang, W.** Multidisciplinary studies of deep Earth: from geodynamo to geodesy, Global Tect. Metal. 8, 113-123, 2003.
- Kutina, J. and **P.T. Taylor**, Satellite altitude magnetic anomalies implications for mineral exploration -A review, Global Tectonics and Metallogeny, vol. 8, nos. 1-4, p.89-106.
- Kutina, J. and **P.T. Taylor**, Introduction, Global Tectonics and Metallogeny, vol. 8, nos. 1-4, p.3-8, 2003.
- Litvak, M. L., I. G. Mitrofanov, A. S. Kozyrev, **D. E. Smith**, et. Al., Seasonal neutron-flux variations in the polar caps of Mars as revealed by the Russian HEND instrument onboard the NASA 2001 Mars Odyssey spacecraft, Solar Syst. Res., 37 (5): 378-386, 2003.
- Liu, H. S., R. Kolenkiewicz** and **C. Wade**, Insolation pulsation theory for atmospheric greenhouse gas concentrations, Recent Research Developments in Atmospheric Sciences, 3, 57-79, 2003a.
- Liu H. S., R. Kolenkiewicz** and **C. Wade Jr.**, Orbital noise of the Earth causes intensity fluctuation in the geomagnetic field, Fluctuation and Noise Lett. 3, L63-L72, 2003b
- Liu, H. S., R. Kolenkiewicz**, J. L. Li and J. Z. Chen, Satellite detection of the convection generated stresses in Earth, Recent Research Developments in Geophysics, 5, 117-137. 2003.
- Luthcke, S.B., N.P. Zelensky, D.D. Rowlands, F.G. Lemoine**, and **T.A. Williams**, The 1-centimeter orbit: JASON-1 precision

orbit determination using GPS, SLR, DORIS and altimeter data, *Marine Geodesy*, Vol. 26, pp. 399-421, 2003

Lyapustin, A., Interpolation and Profile Correction (IPC) method for shortwave radiative transfer in spectral intervals of gaseous absorption. *J. Atmos. Sci.*, 60, 865-871, 2003.

Mitrofanov, I. G., M. T. Zuber, M. L. Litvak, **D. E. Smith**, et. al. CO₂ snow depth and subsurface water-ice abundance in the northern hemisphere of Mars, *Science* 300 (5628): 2081-2084, 2003.

Neumann, G. A., D. E. Smith, and M. T. Zuber, Two Mars years of clouds detected by the Mars Orbiter Laser Altimeter, *J. Geophys. Res.-Planets*, 108 (E4): no. 5023, 2003.

Petrov, L. and C. Ma, Study of harmonic site position variations determined by VLBI, *J. Geophys. Res.*, vol. 108, No. B4, 2190, doi: 10.1029/2002JB001801, 2003.

Purucker, M., Review of: Surface Exploration Case Histories: Applications of Geochemical, Magnetic, and Remote Sensing Methods to Exploration, Field Development, and Production, edited by Dietmar Schumacher and Leonard LeSchack, ISBN, AAPG / SEG, Tulsa, 2002, The Leading Edge, vol 22, no.8, pages 790 and 800, 2003.

Ray, R. D. and B. D. Beckley, Simultaneous ocean wave measurements by the Jason and Topex satellites, with buoy and model comparisons, *Marine Geodesy*, 26, 367-382, 2003.

Ray, R. D. and R. M. Ponte, Barometric tides from ECMWF operational analyses, *Annales Geophysicae*, 21, 1897-1910, 2003.

Ray, R. D., D. D. Rowlands, and G. D. Egbert, Tidal models in a new era of satellite gravimetry, *Space Science Reviews*, 108, 271-282, 2003.

Rubincam, D. P., Polar wander on Triton and Pluto due to volatile migration, *Icarus*, 163, 469-478, 2003.

Rubincam, D. P., Gravitational core-mantle coupling and the acceleration of the Earth, *J. Geophys. Res.*, 108, B7, 2338, doi:1029/2002JB002132, 2003.

Sanchez, B. V., D. D. Rowlands, R. M. Haberle, and J. Schaeffer, Atmospheric rotational effects on Mars based on the NASA Ames general circulation model, *J. Geophys. Res.*, Vol. 108, NO. E5, 5040, doi:10.1029/2002JE001984, 2003.

Solomon, S., V. R. Baker, J. Bloxham, J. Booth, A. Donnellan, C. Elachi, D. Evans, E. Rignot, D. Burbank, **B. Chao**, A. Chave, A. Gillespie, T. Herring, R. Jeanloz, J. LaBrecque, B. Minster, W. Pitman, M. Simons, D. L. Turcotte, and Zoback, M. L., 2003, Plan for living on a restless planet sets NASA's Solid Earth agenda: EOS (Transactions of the American Geophysical Union), v. 84, p. 485-492.

Taylor, P. T. and J. J. Frawley, Satellite altitude magnetic data and the search for mineral resources-The Kiruna region, Sweden, *Global Tectonics and Metallogeny*, vol. 8, nos. 1-4, p. 165-178, 2003.

Taylor, P. T., J. J. Frawley, H. R. Kim, R. von Frese and J. W. Kim, Comparing Magsat, Ørsted and CHAMP crustal magnetic anomaly data over the Kursk Magnetic Anomaly, Russia, First CHAMP Mission Results for Gravity, Magnetic and Atmospheric Studies, Eds. C. Reigber, H. Luhr and P. Schwintzer, Springer, p. 302-308, 2003.

Vennerstrom, S., N. Olsen, **M. Purucker**, M. H. Acuna, and J. C. Cain, The magnetic field in the pile-up region at Mars, and its variation with the solar wind, *Geophys. Res. Lett.*, 30(7), 1369, doi: 10.1029/2003GL016883, 2003.

von Frese, R. R. B., H. R. Kim, **P. T. Taylor** and J. W. Kim, CHAMP, Ørsted, and Magsat Magnetic Anomalies of the Antarctic Lithosphere, First CHAMP Mission Results for Gravity, Magnetic and Atmospheric Studies, Eds. C. Reigber, H. Luhr and P. Schwintzer, Springer, p. 309-314, 2003.

Whaler, K., and **M. Purucker**, Martian magnetization-preliminary models, *The Leading Edge*, 22(8), 763-765, August, 2003.

Proceedings Papers, NASA Technical Documents, etc.

Ciufolini, I. and **E. C. Pavlis** The gravitomagnetic field and its measurement with the LAGEOS satellites, Proceedings of the 3rd William Fairbank Meeting on the Lense-Thirring Effect, June 29 -- July 4, 1998, Rome, R. Ruffini and C. Sigismondi (eds.), World Scientific, Singapore, pp. 185-200, 2003.

Carabajal, C.C., D.J. Harding, J.L. Bufton, S.B. Luthcke and **D.D. Rowlands**, ICESat Geolocation and Land Products Validation: Laser Altimetry Profile and Waveform Matching, ISPRS workshop on 3D mapping from InSAR and Lidar, Portland OR, June 17-19, 2003.

Heirtzler, J.R., The Geomagnetic Field During a Reversal, NASA/TM-2003-212250, 7 p

Kim, H.R., R.R.B. von Frese, **P.T. Taylor**, J.W. Kim and C. H. Park, Utility of satellite magnetic observations for estimating near-surface magnetic anomalies, OIST-4 Proceedings, 4th Oersted International Science Team Conference, p. 83-86, 2003.

Luthcke, S. B., D. D. Rowlands, C. C. Carabajal, D. J. Harding, J. L. Bufton and **T. A. Williams**, ICESat laser altimeter pointing, ranging and timing calibration from integrated residual analysis: a summary of early mission results, Proceedings of the Flight Mechanics Symposium, NASA Goddard Space Flight Center, Oct. 28-30, 2003.

Luthcke, S. B., D. D. Rowlands, F. G. Lemoine, N. P. Zelensky and **T. A. Williams**, GPS-based precision orbit determination for a new era of altimeter satellites: Jason-1 and ICESat, Proceedings of the Flight Mechanics Symposium, NASA Goddard Space Flight Center, Oct. 28-30, 2003.

MacMillan, D. S., Quasar apparent proper motion observed by geodetic VLBI networks, Proceedings of Future Directions in High Resolution Astronomy: The 10th Anniversary of the VLBA, Socorro NM, June 2003.

Mertikas, S. P., **E. C. Pavlis** and P. Drakopoulos GAVDOS: A satellite radar altimeter calibration and sea-level monitoring site on the island of Gavdos, Crete, H. Dahlin, N. C. Flemming, K. Nittis, S. E. Pettersson (eds.), EC Operational Forecasting Workshop: Reports on the EC of Projects, Proceedings of the 3rd EuroGOOS Conference, 3-6 December 2002, Athens, Greece, Elsevier Oceanography Series, 69, 8 pages, (in press 2003).

Mertikas, S. P., **E. C. Pavlis**, P. Drakopoulos and K. Palamartchouk A European radar altimeter calibration and sea-level monitoring site for JASON-1 and ENVISAT at the island of Gavdos, Crete, Greece, C. R. Rostater, Jr. and R. Santoleri (eds.), Remote Sensing of the Ocean and Sea Ice 2002, Proceedings of SPIE, Vol. 4880, pp. 52-59, 2003

Niell A., and **L. Petrov**, Using a numerical weather model to improve geodesy, Proceedings of The State of GPS Vertical Positioning Precision: Separation of Earth Processes by Space Geodesy, Luxemburg, April 2003.

Pavlis, E. C., Monitoring the origin of the TRF with space geodetic techniques, Proceedings of the 13th International Laser Ranging Workshop, (eds. Klosko, Noll and Pearlman), Washington DC, USA, October 7-11, 2002, NASA CP 2003-212248, Greenbelt, MD, 2003.

Petrov, L. Contribution of the VLBA network to geodynamics, Proceedings of Future Directions in High Resolution Astronomy: A Celebration of the 10th Anniversary of the VLBA, Socorro, June 2003.

Petrov, L., D. Gordon, A. Beasley, E. Fomalont, VLBA calibrator survey: astrometric and image results, Proceedings of Future Directions in High Resolution Astronomy: A Celebration of the 10th Anniversary of the VLBA, Socorro, June 2003.

Purucker, M., T. Sabaka, N. Olsen, and S. Maus, How have Oersted, CHAMP, and SAC-C improved our knowledge of the oceanic regions, OIST-4 Proceedings, 4th Oersted International Science Team Conference, 89-95 (2003).

Purucker, M. and N. Olsen, Modeling of the Earth's magnetic field and its variation with Oersted, CHAMP, and Oersted-2/SAC-

C, OIST-4 Proceedings, 4th Oersted International Science Team Conference, 319-327 (2003).

Stauning, P., H. Luhr, P. Ulte-Guerard, J. LaBrecque, **M. Purucker**, F. Primdahl, J.L. Jorgensen, F. Christiansen, P. Hoeg, K.B. Lauritsen, (editors). OIST-4 Proceedings, 4th Oersted International Science Team Conference, 2003, DMI Scientific Report 03-09, Copenhagen, 370 pp. (2003)

Smith, D. E. and M. T. Zuber, Seasonal changes in the masses of the polar icecaps of Mars derived from Mars Global Surveyor gravity, Proceedings of the Mars Atmosphere Modeling and Observations Workshop, Granada, Spain, January 13-15, 2003.

Smith, D. E. and M. T. Zuber, Modeling the changes in mass of Mars' seasonal polar icecaps with gravity, Proceedings of the European Geophysical Society / American Geophysical Union's Joint Assembly meeting, Nice, France, April 6-11, 2003.

Taylor, P.T., H.R. Kim, R. R.B. von Frese, L.V. Potts and J.J. Frawley, Satellite-Altitude Geopotential study of the Kursk magnetic Anomaly (KMA), OIST-4 Proceedings, 4th Oersted International Science Team Conference, p. 95-98, 2003.